The $\nu 4$ bands at 11 μm: linelists for the Trans- and Cis-conformer forms of nitrous acid (HONO) in the 2019 version of the GEISA database

Raymond Armante, Agnès Perrin, F. Kwabia Tchana, L. Manceron

The ν4 bands at 11 µm: linelists for the Trans- and Cis- conformer forms of nitrous acid, (HONO), in the 2019 version of the GEISA database

R.Armante[a], A.Perrin[a],

F. Kwabia Tchana [b],

L. Manceron [c,d],

[a]Laboratoire de Météorologie Dynamique/IPSL, UMR CNRS 8539, Ecole Polytechnique, Université Paris-Saclay, RD36, 91128 Palaiseau Cedex, France

.[c] Ligne AILES, Synchrotron SOLEIL, L'Orme des Merisiers, St-Aubin BP48, 91192 Gif-sur-Yvette Cedex, France.

[d]Sorbonne Université, CNRS, MONARIS, UMR 8233, 4 place Jussieu, Paris, F-75005 France

[b] Université de Paris and Univ Paris Est Creteil, CNRS, LISA, F-75013 Paris, France

Nb of Tables: 3

Nb of Figures: 4

Keywords: IASI-NG, GEISA, Trans-HONO, Cis-HONO, 11µm.

Abstract

Using line positions and line intensies parameters existing in the literature for the Trans- and Cis conformer forms of nitrous acid (HONO), we generated for the first time a linelist of positions, intensities, and line shape parameters for the ν_4 bands of nitrous acid located at 790.117 cm^{-1} and 851.943 cm^{-1} for the Trans- and Cis- conformers, respectively. A validation of this linelist was performed using spectra recorded by the IASI (Interféromètre Atmosphérique de Sondage Infrarouge) satellite instrument in February 2009 during the (rather) exceptional conditions of the large Australian bush fires. This list, which is now included in the 2020 version of the GEISA database (https://geisa.aeris-data.fr/) is of potential interest for the *IASI-NG* (Infrared Atmospheric Sounding Interferometer - New Generation) instrument which will be launched on board the METOP-SG satellite in 2021.

I Introduction

Nitrous acid (HONO) plays an important role in the production of photochemical smog. This species which accumulates at night [1] dissociates quickly by subsequent photolysis at sunrise. The photolysis of HONO is a direct source of hydroxyl radical:

$$\text{HONO} + \text{h}\nu(\lambda < 400 \text{ nm}) \rightarrow \text{OH} + \text{NO}. \qquad \text{Eq. (1)}$$
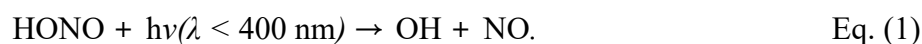
The OH radical is a key species in the photochemical cycles responsible for tropospheric ozone formation, leading to the so called ''photochemical smog'' in polluted area. Biomass burning is a significant global source of trace gases and particles in the atmosphere. Among others, nitrous acid (HONO) has been observed in biomass burning plumes [2, 3].

As far as optical methods are considered, atmospheric gas phase concentrations of nitrous acid can be measured in situ by long path differential optical absorption spectroscopy (DOAS) in the near UV region [4], by Tunable Diode Laser Absorption Spectroscopy [5], by FTIR spectroscopy [2]. However, contrary to what can potentially be achieved from a satellite, these measurements cannot provide easily an overview at the scale of the Earth on the concentration of this species.

Recently Clarisse et al. [6] provided an overview of several trace gases than can be observed by the Infrared Atmospheric Sounding Interferometer (IASI) instrument [7] during the (rather) exceptional conditions of the large Australian bush fires of February 2009. On this occasion HONO could be detected for the first time from a satellite instrument in the 11 µm region. Considering that the fires were even more violent during the late 2019- to early 2020 period, HONO may be detectable in atmospheric spectra recorded over Australia.

The three IASI instruments are thermal infrared nadir[1] Fourier Transform Spectrometer (operating in the 3.5 - 15.5 µm spectral range) which are implemented on the series of METOP satellites. Very soon, the IASI instruments will be followed by the Infrared Atmospheric Sounding Interferometer New Generation (IASI-NG; https://iasi-ng.cnes.fr/fr). IASI-NG is a key payload element of the second generation of European meteorological polar-orbit satellites (METOP-SG) dedicated to operational atmospheric nadir soundings. For IASI-NG the performance objective is mainly a spectral resolution and a radiometric error divided by two compared with the IASI first generation ones. One can presume that the possible quantification of trace species from space like HONO will be easier by IASI-NG than by IASI. It is important to prepare and optimize such detection in order to take full advantage of the future capacities of IASI-NG.

The 11 µm region for HONO

Nitrous acid (HONO), exists in two conformer forms (Cis and Trans), and the 11 µm region which corresponds to the v_4 bands for both conformer forms, is particularly suitable for the detection of this species by IASI or IASI-NG. This rather strong signature, with two narrow Q-branches, located at 790.117 and 851.943 cm^{-1} for the Trans- and Cis- conformers, respectively, corresponds to a rather clear window of transparency in the Earth atmosphere. However, up to now there exists no line by line spectroscopic parameters for this species in common access databases [8, 9]. Accordingly, the HONO detection performed by Clarisse et

---

[1] Nadir is the downward-facing viewing geometry of an orbiting satellite during remote sensing of the atmosphere.

al. [6] was performed using the HONO infrared cross sections available at a nominal temperature of 296K in the Pacific Northwest National Laboratory (PNNL) database [10].

These PNNL parameters [10] are a compilation of laboratory Fourier transform spectra recorded at the optimum resolution of 0.06 cm^{-1} for different mixture of HONO with other gases [11]. The main disadvantage of using cross sections for the retrieval process is that these laboratory data cannot reproduce the HONO infrared signature in all the different physical conditions encountered by the optical signal along its path in the atmosphere during satellite sounding (very long optical path length, temperature and pressure of the different gas components).

The future detections of this species by IASI-NG may concern HONO in the troposphere at night, (or/and) in the plume of bush fires. It is important to make the difference between the two types of signatures. The goal of the present study was to generate the first line by line list of spectroscopic parameters for HONO in the 11 μm region, which is now implemented in the 2020 version of the GEISA database (https://geisa.aeris-data.fr/). Likely, the possible temperature dependence of the HONO infrared signature in atmospheric conditions can be evidenced when using these line by line parameters.

II Existing line parameters for the ν_4 bands of Trans- and Cis- HONO (nitrous acid).

For the present task, we relied on the existing line position, line intensity and line shape parameters collected in the literature.

A. Line positions

To our knowledge the most extensive spectroscopic line position investigation of the ν_4 fundamental bands of Trans-HONO and Cis-HONO was performed by Kleiner et al. [12] using high resolution Fourier transform spectra. The lines assigned for the ν_4 bands of both conformer forms were fitted using A- type and S-type Watson's type Hamiltonians, giving rise to a set vibrational and rotational parameters for the ground states and 4^1 excited states of these conformer species. Later on, the ground state of HONO rotational parameters were refined during the investigation of the far infrared spectrum of HONO performed in Ref. [13].

B Line intensities

To compute line intensity parameters for the ν_4 fundamental bands of Trans-HONO and Cis-HONO, it is necessary to have at our disposal their associated transition moment operator, $^{Trans,4}\mu_Z$ and $^{Cis,4}\mu_Z$, respectively.

To our knowledge, there exists no individual line intensity measurements in the literature, for the ν_4 bands of Trans-HONO or Cis-HONO. Therefore the parameters involved in the expansion of $^{Trans,4}\mu_Z$ and $^{Cis,4}\mu_Z$ can only be obtained by scaling performed on the existing band intensities of the ν_4 bands of Trans-HONO and Cis-HONO. Getting "absolute experimental intensities" for HONO requests to know the "absolute" concentration (or partial pressure) of Trans-HONO and Cis-HONO present in the cell during the recording of the laboratory spectra. This information is not easily available since one has to face difficulties linked to (i) the non-chemical purity in HONO and (ii) the existence of two conformers (Trans- and Cis- for HONO)

a. Chemical purity in nitrous acid (HONO)

In usual laboratory conditions, nitrous acid exists only in the form of an equilibrium mixture with other species like NO, NO_2 and H_2O, together with smaller quantities of N_2O_3, N_2O_5, and HNO_3 [11]. The first spectroscopic works on HONO were performed, relying on the equilibrium constants of complex reactions system of NO, NO_2, and water to determine the partial pressure of nitrous acid in the gas sample present in the cell during the spectra recording [11, 14, 15, 16, 17]. Accordingly, all these reported line strengths are directly dependent on the accuracy of these equilibrium constants.

In 1995 Becker at al. [18] measured line intensities for the ν_3 H-O-N bending mode of trans-HONO near 1255 cm^{-1}, and in this case high purity HONO (> 98%) was produced by a reaction of gaseous HCl with solid $NaNO_2$. Such method was also used by Barney et al. [19] and during the infrared absorption cross sections measurements of HONO, the spectra were recorded by combining simultaneously UV/visible and FTIR spectroscopy. However, this chemical technique is not so straightforward to use, as the molecules are produced in a nitrogen buffer gas flow in a moist atmosphere and implies a delicate control of the reactions equilibrium constants to avoid excessive NO, NO_2 and HNO_3 production and the knowledge of the nitrogen and water pressure broadening coefficients. It was not used during the investigations of the 11 µm region [11], and the cross sections delivered by the Pacific Northwest National Laboratory (PNNL) [10] are calibrated in absolute relative to the intensity data achieved in Ref. [11].

b. Trans- and Cis- conformer forms for HONO

The temperature dependence of the Cis- to Trans- population ratio, $r_T^C(T) = \left(N_{Cis} \big/ N_{Trans} \right)(T)$ is directly related to the difference energy $\Delta E_{Cis\text{-}Trans}$ between the ground vibrational states of the Cis and Trans-conformer forms:

$$r_T^C(T) = \left(N_{Cis} \big/ N_{Trans} \right)(T) = \exp\left(-\Delta E_{Cis-Trans} \big/ kT \right) \qquad \text{Eq.(2)}$$

As a consequence, the partial pressure of HONO (P_{HONO}) present in the cell involves a contribution from the Trans- and Cis- conformers ($P_{HONO} = P_{Trans} + P_{Cis}$). According to Eq. (1) these entities are related by the following equation:

$$P_{Trans}(T) = P_{HONO} \times \left(1 \big/ \left(1 + r_T^C(T) \right) \right),$$

$$P_{Cis}(T) = P_{HONO} \times \left(r_T^C(T) \big/ \left(1 + r_T^C(T) \right) \right) \qquad \text{Eqs.(3)}$$

The same equations link the $N_{Trans}(T)$ and $N_{Cis}(T)$ Trans- and Cis- concentrations to the total (Trans and Cis) N_{HONO} concentrations.

Therefore, for a given band of Trans-HONO [16] (resp. of Cis- HONO [15]), the "absolute" band intensity can be quoted in the literature, either relative to the partial concentration $N_{Trans}(T)$ (resp. $N_{Cis}(T)$) of the considered conformer, or to the total $N_{HONO}(T)$ HONO concentration. Both types of definitions were used for the band intensity values which are given for the ν_1, ν_2, ν_3, ν_4 and $2\nu_2$ bands of Trans-HONO and ν_1, ν_2, ν_4 and $2\nu_2$ bands of Cis-HONO in Ref. [11]. In this work, we decided to generate a HONO line list which is scaled to the total HONO pressure ($P_{HONO}(T)$) or concentration ($P_{HONO}(T)$) .

$$P_{HONO}(T) = P_{Trans}(T) + P_{Cis}(T), \text{ or } N_{HONO}(T) = N_{Trans}(T) + N_{Cis}(T) \qquad \text{Eq.(4)}$$

This is justified because the "total" HONO (both Trans- and Cis-) concentration is the entity which is requested for atmospheric applications. Furthermore, in actual atmospheric conditions, the Cis- to Trans- population ratio, is expected to depend on the temperature at the considered altitude.

We have to adopt a reliable value for $\Delta E_{\text{Cis-Trans}}$ since this entity, which was determined during several experimental [20, 21, 22, 23, 24] and ab initio [25, 26, 27, 28, 29] investigations, is not firmly established. At the present time we are unable to decide which value of $E_{\text{Cis-Trans}}$ is the correct one.

Among these, various experimental values range from 107 to 225 cm^{-1}. The most recent study by Sironneau et al. [24] which has led to:

$$^{\text{S}}E_{\text{Cis-Trans}} = 107 \pm 26 \text{cm}^{-1} \qquad \text{Ref. [24]} \qquad \text{Eq.(5)}$$

was obtained during the investigation of the far infrared spectra of HONO and DONO, and this value of $E_{\text{Cis-Trans}}$ leads to $^{\text{S}}r_T^C(T = 296K) \approx 0.594$ for the population ratio.

Let us mention that Kagann and Maki [11] or Barney et al. [19] adopted different "a priori" values for the $r_T^C(T)$ population ratio of the Cis and Trans conformer forms, and these correspond to the following assumed values for $E_{\text{Cis-Trans}}$:

$$^{\text{KM}}r_T^C(T = 296K) \approx 0.5 \qquad \Leftrightarrow \qquad ^{\text{KM}}E_{\text{Cis-Trans}} \approx 143 \text{ cm}^{-1} \qquad \text{Ref. [11]} \qquad \text{Eq. (6)}$$

$$^{\text{B}}r_T^C(T = 296K) \approx 0.43 \quad \Leftrightarrow \quad ^{\text{B}}E_{\text{Cis-Trans}} \approx 171 \text{ cm}^{-1} \qquad \text{Ref. [19]} \qquad \text{Eq.(7)}$$

    c.   *Existing band intensity measurement for the ν_4 bands of Trans- and Cis- for HONO*

To our knowledge, there exist no individual line intensity measurements for HONO in the ν_4 spectral range. Several ab initio band intensities exist for the ν_4 bands of the Trans- and Cis- conformer forms in the literature (see Ref. [30] and references therein), which compare reasonably well with the existing experimental values. As far as the experimental data are concerned, [11, 19, 10], it appears that the band intensity measured at 11 µm by Barney et al. [19] are in rather reasonable agreement with those achieved in Ref. [11]. The PNNL (Pacific Northwest National Laboratory) cross sections [10] which are calibrated in absolute relative to Kagann and Maki band intensities values [11], present the advantage to provide a medium resolution (R~0.11 cm-1) description of the HONO band structure at 11 µm.

Therefore, the present linelist was generated by calibrating the intensities relative the PNNL cross sections in the 11 μm region. To enable an easier comparison with these earlier studies, the Cis-Trans difference energy value $^{KM}E_{Cis\text{-}Trans} \approx 143$ cm^{-1} (Eq. (5)), adopted in Ref. [11], was used during this work as "a priori" value. This choice which is justified (only) by technical reasons, does not prevail over the scientific value that have to be used for $^{KM}E_{Cis\text{-}Trans.}$

Another difficulty is to establish a separation between the spectral coverage of the ν_4 bands of the Trans- and Cis- HONO conformers. Indeed, in the experimental conditions of recording of the PNNL spectra (HONO sample diluted in 1.013 hPa of nitrogen gas, spectra recorded with a Bruker-66V FTIR spectrometer with an instrumental resolution of ~0.112 cm^{-1}) the ν_4 bands of the Trans- and Cis- HONO conformers are not fully separated (see Fig 1). Therefore, in the 720- 1000 cm^{-1} range, we had to define an approximate cutoff separation, $\sigma_{Cut\text{-}off} \approx 820$ cm^{-1}, between the Trans-ν_4 band (centered at 790 cm^{-1}) and the Cis-ν_4 (centered at 852 cm^{-1}). This cutoff value was already used in Ref. [19] for the validation of their results relative to those of Ref. [10].

Using the PNNL cross sections, the following values:

$$\sigma^{<820}S(296K)=1.436 \times 10^{-17}$$
$$\text{and } \sigma^{>820}S(296K)=1.400 \times 10^{-17} \text{ (in cm}^{-1}/(\text{molecule.cm}^{-2}) \qquad \text{Eq.(8)}$$

were achieved for the integrated band intensities for the 720-820 cm^{-1} and 820-920 cm^{-1} regions, respectively. These spectral ranges correspond, more or less, to the ν_4 bands of the Trans- and Cis conformers, respectively, together with their associated hot bands.

C Line shape parameters

Except for tentative air- broadening half width measurements performed in Ref. [18], the line shape parameters are, to our knowledge, absent in the literature for HONO.. The permanent dipole moments of Trans- and Cis-HONO have values, $^{Trans}\mu_0=1.930$ D and $^{Cis}\mu_0=1.428$ D, respectively [31], and these values are similar to the water permanent dipole value ($^{Trans}\mu_0=1.855$ D [32]). For this reason, it was decided to use for the HONO line shape parameters "a priori" values similar to those of water. More explicitly, the values

$$\gamma_{Air}=0.1 \text{ cm}^{-1}/\text{Atm}, \gamma_{Self}=0.4 \text{ cm}^{-1}/\text{Atm}, \text{ and } n_{Air}=0.7 \qquad \text{Eqs. (9)}$$

were implemented for the air-broadened half width, self-broadened half halfwidth and for the n-temperature dependent coefficient, respectively.

III Generation of line positions and line intensities list for Trans- and Cis- HONO

   A. Line positions:

As usual, the line positions of the ν_4 bands are the differences between the upper and lower state energy levels. The $\left[J \ , K_a , K_c \right]$ and $\left[J' , K_a' , K_c' \right]$ energy levels in the ground and 4^1 vibrational states of HONO, respectively were computed using an A-type and I^r Watson's type Hamiltonian and using the vibrational energies and the rotational constants quoted in Tables 1 and 2, for the Trans- and Cis- conformers respectively. As far as the ground state is concerned, these constants are those determined recently by Dehayem et al. [13], which are presumed to be more accurate than those quoted in Ref. [12]. For the upper 4^1 state, the rotational constants were marginally readjusted from those achieved by Kleiner et al. [12] using the following expression

$$^{New}X_4 = \left(^{Kleiner}X_4 - \ ^{Kleiner}X_0 \right) + \ ^{Dehayem} X_0 \qquad \text{Eq. (10)}$$

In this expression, $^{Kleiner}X_4$ and $^{Kleiner}X_0$ are the rotational or centrifugal constants for the ground and 4^1 excited stated quoted in Ref. [12], while $^{Dehayem}X_0$ is the corresponding ground state value in Ref. [13].

For usual molecules, the line by line list in spectroscopic databases [8,9] possess one column which gives, for each of a given $\left[J' , K_a' , K_c' \right]$- $\left[J \ , K_a , K_c \right]$ transition, the value $E_{Lower}(J, K_a, K_c)$ of the lower-state energy.

For this line list, the lower state energy levels for both HONO conformers are defined relative to the position of the J=0 level of the Trans- conformer. This means that the values

$$^{Trans}E_{Lower}(J, K_a, K_c) = {}^{Trans}E_{Rot}(J, K_a, K_c) \qquad \text{Eq.(11,a)}$$

$$\text{and} \qquad {}^{Cis}E_{Lower}(J, K_a, K_c) = {}^{KM}E_{Cis\text{-}Trans} + {}^{Cis}E_{Rot}(J, K_a, K_c) . \qquad \text{Eq.(11,b)}$$

are quoted for the Trans- and Cis- conformers, respectively. This is because the J=0 lower rotational energy level in the ground vibrational state of the Cis-Conformer form is located at $^{KM}E_{Cis\text{-}Trans} \approx 143$ cm^{-1} above its Trans- counterpart.

B. Line intensities:

As pointed out later in the text, the line intensities computation is subject to numerous uncertainties and possible large systematic errors. Therefore, during this study we will neglect the difference between intensities provided for a "natural sample" to those given for a "pure sample" of $H^{16}O^{14}N^{16}O$. Indeed, this major isotopic species, $H^{16}O^{14}N^{16}O$, is present with a rather high concentration ($I_a = 0.9914$) in a "natural sample" of HONO.

B-1 Definitions

For the Trans- HONO conformer form, the intensity of a given line is given (in cm^{-1}/(molecule.cm^{-2}) by [8,9]:

$$^{Trans}k_{\tilde{\nu}}^{N}(T) = \frac{8\pi^3\tilde{\nu}}{4\pi\varepsilon_0\,3hc\,^{Tot}Z(T)}\,g_{nucl}\left(1 - \exp\left(-\frac{hc\tilde{\nu}}{kT}\right)\right)\,\exp\left(-\frac{hcE_A}{kT}\right)\,R_A^B$$

$$\text{Eq.(12)}$$

while for the Cis- conformer form, we used a slightly different expression:

$$^{Cis}k_{\tilde{\nu}}^{N}(T) = \exp\left(-\frac{hc\Delta E_{Cis-Trans}}{kT}\right)\frac{8\pi^3\tilde{\nu}}{4\pi\varepsilon_0\,3hc\,^{Tot}Z(T)}\,g_{nucl}\left(1 - \exp\left(-\frac{hc\tilde{\nu}}{kT}\right)\right)\,\exp\left(-\frac{hcE_A}{kT}\right)\,R_A^B$$

$$\text{Eq.(13)}$$

Indeed, for the Cis- conformer, Eq.(13) includes the " $\exp\left(-\dfrac{hc\Delta E_{Cis-Trans}}{kT}\right)$ " term to account

for the definition of the J=0 level of the Cis- conformer relative to the Trans- one.

It is necessary to detail the different terms which appear in the right hand side of Eqs. (12) and (13).

- The subscripts A and B are for the lower and upper levels of the transition, respectively, and , $\widetilde{v}=(E_B-E_A)/hc$ is the wavenumber of the transition, and the $^{Trans}E_A(J, K_a, K_c)$ and $^{Trans}E_B(J, K_a, K_c)$ (resp. the $^{Cis}E_A(J, K_a, K_c)$ and $^{Cis}E_B(J, K_a, K_c)$) lower and upper state energy levels are computed using the parameters quoted in Table 1 for Trans- HONO (resp. in Table 2 for Cis-HONO), and respectively.

- g_{nucl} is the nuclear spin factor which is set to a constant value (g_{nucl} =1) for all rotational levels of the Cis- and Trans- HONO and will be omitted in the rest of the discussion.

- $^{Tot}Z(T)$ is the "total" partition function of HONO at the temperature T, which includes a contribution from the Trans- and Cis- conformers, $^{Trans}Z_{Tot}(T)$ and $^{Cis}Z_{Tot}(T)$, respectively.

$$^{Tot}Z(T)=^{Trans}Z(T)+^{Cis}Z(T) \qquad \text{Eq. (14)}$$

For each conformer, these contributions are computed as usual [33] in the Harmonic Oscillator Approximation (HOA as the product of its vibrational and rotational contributions. These individual vibrational contributions were computed using the usual expressions, with for example for the Trans- form:

$$^{Trans}Z_{Vib}(T)= \prod_{i=1-6}(1-\exp(hc\omega_i / kT))^{-1} \qquad \text{Eq. (15)}$$

where, the i- product is performed on the six (non-degenerate) vibrational fundamental modes of Trans-HONO [16, 34] or Cis- conformer form [15, 34, 20].

For the Trans form, $^{Trans}Z(T)$ is written as:

$$^{Trans}Z(T)=^{Trans}Z_{Vib}(T)\times ^{Trans}Z_{Rot}(T) \qquad \text{Eq. (16)}$$

with, as usual :

$$^{Trans}Z_{Rot}(T)= \sum_{all\,rotational\,levels}(2J+1)\exp\left(-hc^{Trans}E_A(J,K_a,K_c)/kT\right). \qquad \text{Eq. (17)}$$

In Eq. (17), the summation in the right hand part of this equation involves the (2J+1) usual factor, where J which is the total rotational quantum number,

For the Cis- conformer, the same equation is written as:

$$^{Cis}Z(T) = {}^{Cis}Z_{Vib}(T) \times {}^{Cis}Z_{C\text{-}T\text{-}Rot}(T),$$ Eq. (18)

Indeed, for the Cis- conformer, the $^{Cis}Z_{C\text{-}T\text{-}Rot}(T)$ rotational contribution takes a different form because of the convention adopted for its J=0 level:

$$
\begin{aligned}
^{Cis}Z_{C-T-ROT}(T) &= \exp\left(-hc\left(\frac{^{KM}E_{Cis-Trans}}{kT}\right)\right) \\
&\times \sum_{(all\ rotational\ levels)}(2J+1)\exp\left(-hc\ ^{Cis}E_A(J,K_a,K_c)/kT\right)
\end{aligned}
$$ Eq. (19)

The results of the $Z_{Tot}(T)$ calculations in the T=70K -340K temperature range are provided as Supplementary data of the present article.

- In Eq. (12) (resp. Eq. (13)), the Trans- (resp. Cis-) R_A^B factors, are the square of the matrix element of the transformed transition moment operator μ_Z' for the Trans- conformer (resp. Cis- conformer). For the Cis- conformer form for example one can write:

$$^{Cis}R_A^B = \left|\left\langle 4^1, J' K'=_a K'_c\left|{}^{Cis,4}\mu_Z\right|0, J'' K''_a K''_c\right\rangle\right|^2$$ Eq.(20)

where $|4^1\rangle$ and $|0\rangle$ are the upper and lower state of the transition, and $^{Cis,4}\mu_Z$ is the Z-component of the ν_4 transformed transition moment operator for the Cis- conformer form [35]. A similar expression can be written for Trans-HONO.

Both the Trans-HONO and Cis-HONO are planar C_s- type molecules, and for symmetry considerations, both A- and B-type transitions are to be observed for the ν_4 bands with ($\Delta K_a = 0$, $\Delta K_c = \pm 1$) and ($\Delta K_a = \pm 1$, $\Delta K_c = \pm 1$) selection rules, respectively, on the K_a and K_c rotational quantum numbers.

In fact, the ν_4 band of Cis-HONO is a hybrid band, and during the investigation of Kleiner et al. [12] weaker B – type transitions were identified together with stronger A-type transitions. On the other hand, for the Trans- conformer form, only A-type transitions were observed. Therefore, up to the first order, one has:

$$^{Cis,4}\mu_Z' = {}^{Cis,4}\mu_1^B \times \varphi_x + {}^{Cis,4}\mu_1^A \times \varphi_z \qquad \text{Eq.(21)}$$

$$^{Trans,4}\mu_Z = {}^{Trans,4}\mu_1^A \times \varphi_z \qquad \text{Eq.(22)}$$

for the Cis- conformer form and Trans- conformer form, respectively. In Eqs. (21) and (22), $\varphi_{x=B}$ and $\varphi_{z=A}$ are the direction cosine between the Z- laboratory fixed and the x=B and z=A molecular fixed axes, respectively.

B-2 Numerical values for the line intensity parameters

To compute the line intensities, one need to estimate the values for the ${}^{Cis,4}\mu_1^A$, ${}^{Cis,4}\mu_1^B$, and ${}^{Trans,4}\mu_1^A$ parameters.

Two types of informations can be used.

First the integrated band intensity ${}^{Trans}S(296K)$ and ${}^{Cis}S(296K)$ in the 720-820 cm^{-1} and 820-920 cm^{-1} (see Eq. 8) were deduced from the PNNL cross sections data. However these integrated band intensity includes contributions from hot bands together with those from the ν_4 cold bands. Therefore each ν_4 cold band contribution, can be estimated from ${}^{Trans}S(296K)$ and ${}^{Cis}S(296K)$ using this expression:

$$^{Trans}Int(\nu_4,T) \approx {}^{Trans}S(11\ \mu m,T)/{}^{Trans}Z_{Vib}(T)$$
$$^{Cis}Int(\nu_4,T) \approx {}^{Cis}S(11\ \mu m,T)/{}^{Cis}Z_{Vib}(T) \qquad \text{Eqs.(23)}$$

In Eqs. (23) ${}^{Trans}Int(\nu_4,T)$ and ${}^{Cis}S(296K)$ are the ν_4 band intensity for the Trans and Cis conformers, which in this work are computed by summing on the ν_4 individual line intensities. At 296K the vibrational partition functions of the Trans and Cis- conformer form differ only marginally. We used for the present work the mean value ($Z_{Vib}(296K)= Z_{Vib}(296K) \approx 1.16738$.

Second, it was stated in Ref. [12] that at room temperature the observed lines for these ν_4 bands are in the intensity ratio of about 1 /0.12/ 1 respectively for A-type lines in the Cis conformer/ B-type lines in the Cis conformer/ A-type lines in the Trans conformer.

Using these informations, and the partitions functions quoted in supplementary data of this paper, we achieved the following values for the $^{\mathrm{Cis},4}\mu_1^A$, $^{\mathrm{Cis},4}\mu_1^B$, and $^{\mathrm{Trans},4}\mu_1^A$ parameters:

$$^{\mathrm{Cis},4}\mu_1^A \approx 0.332 \text{ Debye,} \quad {}^{\mathrm{Cis},4}\mu_1^B \approx 0.115 \text{ Debye, and } {}^{\mathrm{Trans},4}\mu_1^A \approx 0.256 \text{ Debye}$$

Eqs. (24)

In this way, we could perform the computation of the line intensities for the ν_4 bands for Trans- and Cis- conformer form of $H^{16}O^{14}N^{16}O$.

B-3 *Final line intensity computations:*

Table 3 gives the results of the final calculations, together with the comparison with the PNNL experimental data in the 720- 820 cm^{-1} and 820- 980 cm^{-1} spectral range.

Figure 1 gives an overall comparison between the observed PNNL cross sections and the computed cross sections, generated using our linelist. This computation was performed for the experimental conditions defined in the PNNL document [10] (1 ppm-meter of HONO at 296K diluted in one atmospheric pressure of nitrogen, with considerable contamination: NO_2, NO, N_2O, NOCl, CO_2 and H_2O). This document mentioned that the PNNL intensities are scaled to those of Kagann and Maki [11].

IV Discussion

Several points need to be discussed. First, the uncertainties on the line positions and line intensities. Second, it is necessary to quantify the impact of the temperature on the Trans- and Cis- line intensities.

A. Uncertainties

During the line position analysis performed in Ref. [12], the analysis was performed up to rather high rotational quantum numbers and the ν_4 bands appeared as being unperturbed. One may assume an accuracy of ~0.001 cm^{-1} for the positions of the lines involving rotational quantum numbers with $J \leq 50$ and $K_a \leq 16$, and of ~0.002 cm^{-1} for extrapolated computed lines.

On the <u>relative</u> scale we expect the intensities of the Trans- and Cis conformer forms at 296K to be rather consistent, with an uncertainty of 5% on the average, and of 10% for the weaker lines. However we cannot really state on the ratio of the B-type to A-type character for the ν_4 band of Cis-HONO, or on the centrifugal dependence of the transition moment operators for both species. Getting these informations requests that a large set of individual line intensities for the ν_4 bands of the Trans- and Cis species to be measured precisely in the future.

The situation is less satisfactory when dealing with the "absolute" intensities. The intercomparisons performed in experimental papers are clearly uneasy [19, 36]. Owing to the difficulties which were pointed our previously, one may be estimate an overall uncertainty on the absolute intensities between 20% to 30%.

B. <u>Temperature dependence of the line intensities</u>

When looking to Fig. 1, it is clear that the overall signature of the Trans- and Cis-conformer forms look quite similar in strength at 296K (see Eq. (7)). Assuming the $^{KM}E_{Cis-Trans}$ value quoted in Eq. (5), the population of the HONO in the Cis- conformer is about twice smaller than in the Trans- conformer. Consequently, according to our computations, for the ν_4 bands, the square of the transition moment operator associated to the Cis- form is about twice as strong as its Trans counterpart:

$$\left| ^{Cis,4}\mu'_Z \right|^2 / \left| ^{Trans,4}\mu'_Z \right|^2 \approx 1.88 \qquad \text{Eq. (25)}$$

For the cold ν_4 bands of HONO at 11 μm, this has two consequences at low temperature, and, to illustrate this point here, we compare the results at 210K and 296K on Fig. 2:

- At low temperature, the Cis- signature (at 852 cm^{-1}) decreases in strength relative to its Trans- counterpart (at 790 cm^{-1}).

$$^{Cis}Int(\nu_4,210K)/ ^{Trans}Int(\nu_4,210K) \approx 0.772$$
$$^{Cis}Int(\nu_4,296K)/ ^{Trans}Int(\nu_4,296K) \approx 1.025 \qquad \text{Eqs.(26)}$$

The integrated band intensity of HONO at 11 μm S(11 μm,T) is the sum of the line intensities of the cold ν_4 bands for Trans-HONO and Cis-HONO, together with their associated hot

bands (see Eq.(23)). According to our computations, S(11 μm,T) decreases weakly with the temperature, and this is unexpected since this entity is constant for rigid molecules which do not exist in different conformers.

To give an example, we give here the 11 μm band intensities (in 10^{-17} cm^{-1}/(molecule.cm^{-2}) units) at T=210 K and 296 K.

$^{Trans}S(296K)= 1.396$; $^{Cis}S(296K)= 1.431$ and then S(11 μm,296K)= 2.828

$^{Trans}S(210K)= 1.527$; $^{Cis}S(210K)= 1.178E-17$ and then S(11 μm,210K)= 2.705

$$\text{Eqs.(27)}$$

To illustrate these points, Figure 2 compares the 11 μm signatures of HONO at 210 K and 296 K. These two calculations, performed for the same HONO concentration show that, at low temperature (210K), the Q branch structure of the Cis- conformer forms decreases significantly as compared to its Trans counterpart. Such temperature dependence of the Cis versus Trans HONO signature clearly cannot be addressed correctly when the interpretation of the atmospheric spectra [6] is performed using the PNNL cross sections [10].

These unusual temperature effects increase in magnitude with the value of the Cis- to Trans energy difference $\Delta E_{Cis-Trans}$. As a consequence it is clear that future spectroscopic studies must propose a more precise value for this parameter. Indeed, it is presumed that future atmospheric measurements of HONO in the 11 μm region from satellite will use simultaneously the 790 cm^{-1} (Trans) and 852 cm^{-1} (Cis) Q- type signatures for the HONO retrievals. Therefore the Trans- and Cis- line intensities must be consistent with each other, regardless of the temperature.

C. Future possible improvements

As discussed previously it is clear that the main effort should focus on the line intensities.

First it is necessary to have at our disposal really accurate absolute intensities based on the knowledge of the absolute concentration of HONO present in the cell during the recording of the spectra. Several techniques exist in the literature. To give an example, for the

ν_3 band of Trans-HONO, at 1255 cm^{-1}, the Trans-HONO concentrations were determined either by ion chromatography or by a NOx chemiluminescence analyzer [18]. Another solution is to use the line intensity inter-comparison technique between the far- infrared and the 11 μm region. This technique was successfully used for getting absolute intensities for the ν_2 band of HOCl [37].

Second, it is necessary to have reliable value of the energy difference between the Trans- and Cis-conformer form of nitrous acid ($E_{Cis-Trans}$). This was done in the literature (Ref. [24] and references therein) by performing line intensity measurements for Trans-HONO and Cis-HONO rotational transitions at high resolution in the far infrared or Thz region, and by comparing the observed absorptions to the theoretical computed intensities.

V Validation by IASI

Since the new generation of satellite infrared instruments like AIRS (Atmospheric Infrared Sounder, https://airs.jpl.nasa.gov/) [38], IASI [7], the Cross-track Infrared Sounder (CrIS) https://www.jpss.noaa.gov/cris.html [39], the detection (sometimes the inversion) of trace gases has been made available from space. For the first time, HONO has been detected by the IASI instrument during the exceptional conditions of the large Australian bush fires of February 2009 [6].

One objective of instruments like IASI-NG is, with an important improvement of the spectral resolution, as well as the signal to noise ratio, to be able to not only detect these kind of conformer forms, but also to be able at least to determine the total content. It is why determination of line list, as it has been done here, is important.

To verify its constituency, a first preliminary inversion of the HONO total content has been done. The case retained is the same as the event mention in the paper of Clarisse et al (Australian fires in February 2009).

For doing that, the operational release of the **A**utomatized **A**tmospheric **A**bsorption **A**tlas (4A) radiative transfer model (4A/OP) [40] has been adapted. The reference HONO concentration profile has been set to:

- 1.5 ppbv in the Boundary Layer. According to the paper of Michoud et al, [41] this extreme measurement has been recorded during the MEGAPOLI summer campaign (https://cds-espri.ipsl.upmc.fr/megapoli/index.jsp). This is the value we have set between the surface and the first kilometer.

- 10 pptv above the Boundary layer. According to the paper of Zhang et al. [42], this typical value has been observed above the first kilometer.

This profile corresponds to a total content (X_{HONO} in the following) of 20.6 pptv.

For this modelisation we used the "Thermodynamic Initial Guess Retrieval" (LMD/TIGR, (https://ara.lmd.polytechnique.fr/index.php?page=tigr) data set, in its latest version. The LMD/TIGR [43] is a climatological library of 2311 representative atmospheric situations selected by statistical methods from 80,000 radiosonde reports ([44, 45, 46]. Each situation is described, from the surface to the top of the atmosphere, by the values of the temperature, water vapour and ozone concentrations on a given pressure grid. The atmospheres are divided into five airmasses from tropical to cold polar. We used in this study the tropical air mass (so called "mean tropical atmosphere") which corresponds to the largest contamination by water.

The figure 3 (top) shows the result of a simulation of the brightness temperature in the 750- 900 cm^{-1} spectral range with the 4A/OP radiative transfer model , with (in red) and without (in grey) HONO for the Cis/Trans bands. For that simulation, an offset of the initial profile of 50 times is necessary to have a signal above the noise of the IASI instrument (approximately 0.25 K). It corresponds to a total content of HONO (X_{HONO_Ref}) of 1.03 ppbv. In the bottom part of the figure 3 is represented in red the difference between both simulations (with minus without HONO). On blue is represented the sensitivity to a variation of 1% of the water vapor profile. The aim is to find IASI channels sensitive or not sensivite to HONO, and with approximately the same sensitivity to H$_2$O.

According to the results shown on the figure 3, a simple inversion of the IASI spectra (using pairs of channels) has been made to determine the HONO total content.

The total content of HONO has been evaluated using the equation Eq. (28):

$$X_{HONO} = X_{HONO\_Ref} * \sum_{surface}^{Top} \frac{\partial T_b}{\partial \rho_{hono}} * \left(T_b^{obs\_HONO} - T_b^{obs\_baseline} \right)$$

Eq. (28)

With:

- X_{hono_ref} = 1.03 ppbv

- $\frac{\partial Tb}{\partial \rho_{hono}}$ the jacobian with respect to the concentration of HONO (ρ_{hono}) and calculated with 4A/OP

- $T_b^{Obs-HONO}$ corresponds to 2 IASI channels sensitive to HONO (790.25 and 790.5 cm^{-1}).

- $T_b^{Obs-Baseline}$ corresponds to 12 channels between 786 and 789 cm^{-1} not sensitive to HONO and with the same sensitivity to H_2O, aiming to determine the baseline of each spectra with a good precision

To take into account the viewing angle of each IASI observation, the jacobian of HONO has been calculated for different sets of angles from 0 (nadir) to 75 degrees. This method has been applied to the IASI observations over Australia (7 February, 9:30 PM) used in the paper of Clarisse et al and the result is shown on the Figure 4. Due to possible contamination of the surface properties, this evaluation of X_{HONO} has been done only over sea. The values have been plotted in the range 0 to 4 ppbv. The inverted points have been over plotted on a Moderate-resolution Imaging Spectroradiometers (MODIS) image (https://modis-images.gsfc.nasa.gov/products.html) of the same day but at 3 PM.

We can see the good agreement and coherence in the localization of both signals, and, even if the absolute value is not representative due to the hypothesis retained for this inversion and due to the fact that MODIS and IASI not measure in the same spectral range (visible for MODIS and infrared for IASI), a good coherence in the value of the X_{HONO} retrieved. The differences

in the plume shape could be due to the time difference between 3:00 pm and 9:30 pm for the MODIS and IASI observations.

Finally, it is important to mention that this atmospheric study has the only pretention to inform of the coherence of the line list of spectroscopic parameters of HONO described previously.

Supplementary data

The partition function for HONO is provided as supplementary data of the article.

CONCLUSION

During this work, we have generated the first line by line list of spectroscopic parameters for HONO in the 11 μm region which is now in free access on the 2019 version of the GEISA database (https://geisa.aeris-data.fr/). For this task, we used the existing line position and intensity parameters. For the intensities the parameters are based on the existing experimental values for the band intensity of the Trans- and Cis- ν_4 bands at 11 μm. An evaluation of the uncertainties associated to the line positions and intensities was performed. It shows that future laboratory studies should focus on improving the quality of the line intensities parameters. On the relative scale, we expect the line intensities of the ν_4 bands of the Trans- and Cis conformers to be rather consistent. This is not the case for the intensities on an "absolute" scale, which are estimated to be accurate only at 20% to 30%, on the average. This is because our computations are based on laboratory measurements which are complicated by the fact that it is impossible to handle a pure sample of HONO in laboratory conditions. Another remaining uncertainty concerns the height of the barrier between the Cis- and Trans- HONO conformers. The impact of these uncertainties are discussed in the text.

Finally, to have a first atmospheric evaluation of this HONO spectroscopic line list at 11 μm, we have developed a simple inversion method to determine the integrated content of HONO. The result obtained shows a good agreement, especially in the shape of the plume, with what the visible MODIS instrument has independently measured few hours before.

References

[1]U. Platt, D.Perner, G.W. Harris, A.M. Winer and J.N. Pitts Jr. Observations of Nitrous Acid in an Urban Atmosphere by Differential Optical Absorption. Nature **285**, 312–314 (1980).

[2] Yokelson, R. J., Crounse, J. D., DeCarlo, P. F., Karl, T., Urbanski, S., Atlas, E., Campos, T., Shinozuka, Y., Kapustin, V., Clarke, A. D., Weinheimer, A., Knapp, D. J., Montzka, D. D., Holloway, J., Weibring, P., Flocke, F., Zheng, W., Toohey, D., Wennberg, P. O., Wiedinmyer, C., Mauldin, L., Fried, A., Richter, D., Walega, J., Jimenez, J. L., Adachi, K., Buseck, P. R., Hall, S. R., and Shetter, R.: Emissions from Biomass Burning in the Yucatan, Atmos. Chem. Phys., **9**, 5785–5812, doi:10.5194/acp-9-5785, (2009).

 [3] C. E. Stockwell, R. J. Yokelson, S. M. Kreidenweis, A. L. Robinson, P. J. DeMott, R. C. Sullivan, J. Reardon, K. C. Ryan, D. W. T. Griffith, and L. Stevens. "Trace Gas Emissions from Combustion of Peat, Crop Residue, Domestic Biofuels, Grasses, and other Fuels: Configuration and Fourier transform infrared (FTIR) Component of the Fourth Fire Lab at Missoula Experiment (FLAME-4)" Atmos. Chem. Phys., **14**, 9727–9754 (2014).

[4] Yang Wang, Steffen Beirle, Francois Hendrick, Andreas Hilboll, Junli Jin, Aleksandra A. Kyuberis, Johannes Lampel, Ang Li, Yuhan Luo, Lorenzo Lodi, Jianzhong Ma,   Monica Navarro, Ivan Ortega, Enno Peters, Oleg L. Polyansky, Julia Remmers, Andreas Richter,   Olga Puentedura, Michel Van Roozendae, André Seyler, Jonathan Tennyson, Rainer Volkamer, Pinhua Xie, Nikolai F. Zobov, and Thomas Wagner. MAX-DOAS Measurements of HONO Slant Column Densities during the MAD-CAT Campaign: Inter-Comparison, Sensitivity Studies on Spectral Analysis Settings, and Error Budget. Atmos. Meas. Tech., **10**, 3719–3742 (2017).

[5] Schiller, C.L., Locquiao, S., Johnson, T. J., and Harris, G. W.: Atmospheric measurements of HONO by Tunable Diode Laser Absorption Spectroscopy, J. Atmos. Chem., **40**, 275–293, (2001).

[6] L. Clarisse, Y. R'Honi, P.-F. Coheur, D. Hurtmans, and C. Clerbaux, Thermal Infrared Nadir Observations of 24 Atmospheric Gases. Geophys. Res. Res. Lett. **38**, L10802, doi:10.1029/2011GL047271, (2011).

[7] C. Clerbaux, A. Boynard, L. Clarisse, M. George, J. Hadji-Lazaro, H. Herbin, D. Hurtmans, M. Pommier, A. Razavi, S. Turquety, C. Wespes, and P.-F. Coheur. Monitoring of Atmospheric Composition using the Thermal Infrared IASI/MetOp Sounder. Atmos. Chem. Phys., **9**, 6041–6054 (2009).

[8] N. Jacquinet-Husson, R. Armante, N.A. Scott, A. Chédin, L. Crépeau, C. Boutammine, A. Bouhdaoui, C. Crevoisier, V. Capelle, C. Boonne, N. Poulet-Crovisier, A. Barbe, D. Chris Benner, V. Boudon, L.R. Brown, J. Buldyreva, A. Camparguej, L.H. Coudert, V.M. Devi, M.J. Down, B.J. Drouin, A. Fayt, et al. The 2015 edition of the GEISA Spectroscopic Database. J. Quant. Spectrosc. Radiat. Transf. **327,** 31-72 (2016).

[9] I.E. Gordon, L.S.Rothman , C.Hill , R.V.Kochanov, Y.Tan, P.F.Bernath, M.Birk, V. Boudon, A.Campargue, K.V.Chance, B.J.Drouin, J.-M.Flaud, R.R.Gamache, J.T.Hodges, D.Jacquemart, V.I.Perevalov, A.Perrin,   K.P.Shine, M.-A.H.Smith, J. Tennyson, G.C.Toon, H.Tran, V.G.Tyuterev q, A.Barbe q, A.G.Császár, V.M.Devi, T.Furtenbacher, J.J.Harrison, J.-M.Hartmann, A.Jolly, T.J.Johnson, T.Karman, I. Kleiner, A.A.Kyuberis, J.Loos, O.M.Lyulin, S.T.Massie, S.N.Mikhailenko, N. Moazzen-Ahmadi, H.S.P.Müller, O.V.Naumenko, A.V.Nikitin, O.L.Polyansky, M. Rey, M.Rotger, S.W.Sharpe, K.Sung, E.Starikova, S.A.Tashkun, J. Vander Auwera, G.Wagner, J.Wilzewski, P.Wcislo, S.Yu, E.J.Zak. The HITRAN2016 Molecular Spectroscopic Database. J. Quant. Spectrosc. Radiat. Transf. **203** , 3-69 (2017) .

[10] S.Sharpe, T. Johnson, R.Sams, P. Chu, G. Rhoderick, P.Johnson, Gas-phase Databases for Quantitative Infrared Spectroscopy, Appl. Spectrosc. **58**, 1452 (2004).

[11] R. Kagann and A. Maki, Infrared Absorption Intensities of Nitrous Acid (HONO) Fundamental Bands. J. Quant. Spectrosc. Radiat. Transf. **30**, 37-44 (1983).

[12] I. Kleiner, J.-M. Guilmot, M. Carleer, M. Herman, The v_4 Fundamental Bands of Trans- and Cis-HN0$_2$. J. Mol. Spectrosc. **149**, 341–347 (1991).

[13] A. Dehayem-Kamadjeu, O. Pirali, J. Orphal, I. Kleiner, P.-M. Flaud, The far-Infrared Rotational Spectrum of Nitrous Acid (HONO) and its Deuterated Species (DONO) studied by High-Resolution Fourier-Transform Spectroscopy. J. Mol. Spectrosc. **234,** 182–189 (2005).

[14] Deeley, C.M. and I.M. Mills, The Infrared Vibration-Rotation Spectrum of Trans- and Cis-Nitrous Acid, J. Mol. Struct. **100**, 199-213 (1983).

[15] J.-M. Guilmot, F. Mélen, M. Herman, Rotational Parameters for Cis-HONO. J. Mol. Spectrosc. **160,** 401–410 (1993).

[16] J.-M. Guilmot, M. Godefroid, M. Herman, Rotational Parameters for Trans-HONO. J. Mol. Spectrosc. **160,** 387–400 (1993).

[17] M. Herman, J. Vander Auwera, *ULB Report on HONO and N2O4, in ISORAC – Infrared pectroscopy of ozone and related Atmospheric constituents, Air Pollution Research Report 52*, edited by D. Hausamann and J.-M. Flaud, pp. 94-135, ECSC-EC-EAEC, Brussels, (1994).

[18] K.H. Becker, J. Kleffmann, R. Kurtenbach, P. Wiesen, A. Febo, M. Gherardi, R. Sparapani, Line Strength Measurements of Trans-HONO near 1255 cm-1 by Tunable Diode Laser Spectrometry. Geophys. Res. Lett. **22,** 2485-2488 (1995).

[19] W.S. Barney, L.M. Wingen, M.J. Lakin, T. Brauers, J. Stutz, B.J. Finlayson-Pitts, Infrared Absorption Cross-Section Measurements for Nitrous Acid (HONO) at room temperature. J. Phys. Chem. **A 104,** 1692-1699 (2000). ibid. J. Phys. Chem. **A 105,** 4166-4166 (2001).

[20] G.E. McGraw, D.L. Bernitt, I.C. Hisatsune. Infrared Spectra of Isotopic Nitrous Acids. J. Chem. Phys. **45** 1392–1399 (1966).

[21] R. Varma, R.F. Curl, "Study of the Dinitrogen Trioxide-Water-Nitrous Acid Equilibrium by Intensity Measurements in Microwave Spectroscopy", J. Phys. Chem. **80**, 402–409 (1976).

[22] A. Bongartz, J. Kames, F. Welter, U. Schurath, "Near-UV absorption cross sections and Trans/Cis Equilibrium of Nitrous Acid". J. Phys. Chem. **95**, 1076– 1082 (1991).

[23] L.H. Jones, R.M. Badger, G.E. Moore, The Infrared Spectrum and the Structure of Gaseous Nitrous Acid. J. Chem. Phys. **19,** 1599–1604 (1951).

[24] V. Sironneau, J.-M. Flaud, J. Orphal 1, I. Kleiner, P. Chelin. Absolute Line Intensities of HONO and DONO in the Far-Infrared and re-determination of the Energy Difference between the Trans- and Cis-Species of Nitrous Acid. J. Mol. Spectrosc. **259**, 100-104 (2010).

[25] D. Luckhaus, The vibrational Spectrum of HONO: Fully coupled 6D Direct Dynamics https://doi.org/10.1063/1.1567713. J. Chem. Phys. **118**, 8797–8806 (2003).

[26] D. Luckhaus, Multi-Arrangement Quantum Dynamics in 6D: *cis–Trans* Isomerization and 1,3-Hydrogen Transfer in HONO. Chem. Phys. **304**, 79–90 (2004).

[27] Y. Guo, D.L. Thompson, On combining Molecular Dynamics and Stochastic Dynamics Simulations to Compute Reaction Rates in Liquids. J. Chem. Phys. **118**, 1673–1978 (2003).

[28] B.S. Jursic, Density Functional Theory Exploring the HONO Potential Energy Surface. Chem. Phys. Lett. **299**, 334–344 (1999).

[29] F. Richter, M. Hochlaf, P. Rosmus, F. Gatti, H.-D. Meyer, A study of the Mode-Selective Trans–Cis Isomerization in HONO using ab initio Methodology. J. Chem. Phys. **120** 1306– 1317 (2004).

[30] V.P. Bulychev, K.G. Tokhadze, Multidimensional Anharmonic Calculation of the Vibrational Frequencies and Intensities for the Trans and Cis Isomers of HONO with the use of Normal Coordinates.   J. Mol. Structure **708,** 47–54 (2004).

[31] M. Allegrini, J.W.C. Johns, A.R.W. McKellar, P. Pinson, "Stark Spectroscopy with the CO Laser: the ν_2 Fundamental Bands of Trans-and Cis- Nitrous Acid, HNO_2, in the 6 µm region". J. Mol. Spectrosc. **79,** 446–454 (1980).

[32] S.L. Shostak, W.L. Ebenstein, J.S. Muenter, The Dipole Moment of Water. I. Dipole moments and hyperfine properties of H2O and HDO in the ground and excited Vibrational states. J. Chem. Phys. **94**, 5875-5882 (1991). ISSN: 0021-9606, CODEN: JCPSA6

[33] J.Fischer, R.R.Gamache, A.Goldman, L.S.Rothman, A.Perrin, "Total Internal Partition Sums in the 2000 edition of the HITRAN database". J. Quant. Spectrosc. Radiat. Transf. **82,** 401-412 (2003).

[34] A. Perrin, S. Miljanic, A. Dehayem-Kamadjeu, P. Chélin, J. Orphal, J. Demaison. The 14–22 µm Absorption Spectrum of Nitrous Acid studied by High-Resolution Fourier-Transform Spectroscopy: New Analysis of the v_5 and v_6 Interacting Bands of Trans-HONO and first Analysis of the ν_6 Band of Cis-HONO. J. Mol. Spectrosc. **245**, 100–108 (2007).

[35] J.-M. Flaud, C.Camy-Peyret, R.A. Toth, in *Water vapour line Parameters from microwave to medium Infrared (An atlas of $H_2^{16}O$, $H_2^{17}O$ and $H_2^{18}O$ line positions and Intensities between 0 and 4350 cm^{-1}) (*1981), 259 pp. Oxford, UK: Pergamon, Book.

[36] B.H. Lee, E.C. Wood, J. Wormhoudt, J.H. Shorter, S.C. Herndon, M.S. Zahniser, J.W. Munger. Effective Line Strengths of Trans-Nitrous Acid near 1275 cm^{-1} and Cis-Nitrous Acid at 1660 cm^{-1}. J. Quant. Spectrosc. Radiat. Transf. **113**, 1905-1912 (2012).

[37] J. Vander Auwera, J. Kleffmann, J.M.Flaud, G.Pawelke, H. Bürger, D. Hurtmans, R. Pétrisse. Absolute ν_2 Line Intensities of HOCl by Simultaneous Measurements in the Infrared

with a Tunable Diode Laser and Far-Infrared Region Using a Fourier Transform Spectrometer. J Mol Spectrosc. **204,** 36-47 (2000).

[38] H.H. Aumann, M.T. Chahine, C. Gautier, M.D. Goldberg, E. Kalnay, L. M. McMillin, H. Revercomb, P.W.*,* Rosenkranz, W.L. Smith, D.H. Staelin, L.L. Strow, and J. Susskind, AIRS/AMSU/HSB on the Aqua Mission: Design, Science Objectives, Data Products, and Processing Systems*.* Geoscience and Remote Sensing, IEEE Transactions on*,* **41***(2),* 253-264 (2003).

[39] Yong Han, Henry Revercomb, Mike Cromp, Degui Gu, David Johnson, Daniel Mooney, Deron Scott, Larrabee Strow, Gail Bingham, Lori Borg, Yong Chen, Daniel DeSlover, Mark Esplin, Denise Hagan, Xin Jin, Robert Knuteson ,Howard Motteler ,Joe Predina, Lawrence Suwinski, Joe Taylor, David Tobin, Denis Tremblay ,Chunming Wang ,Lihong Wang, Likun Wang, Vladimir Zavyalov, Suomi NPP CrIS Measurements, Sensor Data Record Algorithm, Calibration and Validation Activities, and Record Data Quality. J. of Geophys. Res. **D748**, 12734 – 12748 (2013). Doi:10.1002/2013JD020344, 2013;
https://www.jpss.noaa.gov/cris.html

[40] N. Scott, A. Chédin, A fast line-by-line Method for Atmospheric Absorption Computations: the Automatized Atmospheric Absorption Atlas, J. Appl. Meteor. **20,** 802–812 (1981).

[41] V. Michoud, A. Kukui, M. Camredon, A. Colomb, A. Borbon, K. Miet, B. Aumont, M. Beekmann, R. Durand-Jolibois, S. Perrier, P. Zapf, G. Siour, W. Ait-Helal, N. Locoge, S. Sauvage, C. Afif, V. Gros, M. Furger, G. Ancellet, and J. F. Doussin. Radical Budget Analysis in a Suburban European Site during the MEGAPOLI Summer Field Campaign. Atmos. Chem. Phys., **12**, 11951–11974, (2012).

[42] W. Zhang, S. Tong, M. Ge, J. An, Z. Shi, S. Hou, K. Xia, Y. Qu, H. Zhang, B. Chu, Y. Sun, H. He. Variations and Sources of Nitrous Acid (HONO) during a Severe Pollution Episode in Beijing in Winter 2016". Science of The Total Environment, **648**, 253-262 (2019). https://doi.org/10.1016/j.scitotenv.2018.08.133

[43] F. Chevallier, in *La modélisation du Transfert Radiatif à des Fins Climatiques: Une Nouvelle Approche Fondée sur les réseaux de Neurones Artificiels*. Ph.D. thesis, University Paris VII, (1998), 225 pp. Available from LMD, Ecole Polytechnique, 91128 PalaiseauCedex, France.
https://ara.lmd.polytechnique.fr/index.php?page=tigr

[44] Chédin A., Scott N.A., Wahiche C., Moulinier P.   The Improved Initialization Inversion Method : a High-Resolution Physical Method for Temperature Retrievals from Satellites of the TIROS-N Series.   J. Clim. and Applied Meteor. **24**, 128-143 (1985)

[45] V. Achard . in *Trois Problèmes de l'analyse 3D de la Structure Thermodynamique de l'Atmosphère par Satellite : Mesure du Contenu en Ozone ; Classification des Masses d'Air ; Modélisation Hyper-Rapide du Transfert Radiatif.* PhD thesis, University Paris 7, Avril (1991).

[46] F. Chevallier, F Chéruy, N.A. Scott, and A. Chédin.   A Neural Network Approach for a Fast and Accurate Computation of Longwave Radiative Budget.   J. of Applied Meteorology **37,** 1385-1397 (1998).

List of Tables

Table 1

Trans- HONO

	Ground state [a]	4^1 [b]
E_v		790.117045
A	3.09854472	3.118852068
B	0.417788103	0.415680066
C	$3.67476366 \times 10^{-1}$	0.364985633
Δ_K	9.99541×10^{-5}	1.049526×10^{-4}
Δ_{JK}	1.72610×10^{-6}	1.0462100×10^{-6}
Δ_J	5.10440×10^{-7}	5.0192×10^{-7}
δ_K	3.1076×10^{-6}	3.51545×10^{-6}
δ_J	6.8795×10^{-8}	6.58484×10^{-8}
H_K	0.10200×10^{-7}	0.10655×10^{-7}
H_{KJ}	-0.755×10^{-9}	-0.755×10^{-9}
H_{JK}	-0.629×10^{-10}	-1.6013×10^{-10}
H_J	-0.941×10^{-12}	-1.198×10^{-12}
h_K	-0.109×10^{-8}	-7.9734×10^{-9}
h_{KJ}	-0.89×10^{-11}	-0.89×10^{-11}
L_K	-0.1144×10^{-11}	-0.1144×10^{-11}

Note. The results are in cm^{-1}.

[a] Rotational constants of *Trans*-HONO from Dehayem-Kamadjeu *et al.* [13].
For the 4^1 upper state, the constants were slightly readjusted using the upper and lower states constants from Ref. [12] and the updated ground state parameters from Ref. [13] (see text).

Table 2

Cis-HONO

	Ground state [a]	4^1
E_v		851.943054
A	2.80533545	2.8250760
B	0.439273052	0.436494267
C	0.379067714	0.375629112
Δ_K	6.53248×10^{-5}	6.97493×10^{-5}
Δ_{JK}	-0.28796×10^{-6}	-0.93376×10^{-6}
Δ_J	5.68799×10^{-7}	5.57616×10^{-7}
δ_K	2.82768×10^{-6}	3.38809×10^{-6}
δ_J	9.36594×10^{-8}	9.52723×10^{-8}
H_K	0.5397×10^{-8}	0.5795×10^{-8}
H_{KJ}	-0.678×10^{-10}	-0.7359×10^{-10}
H_J	-0.1078×10^{-11}	-0.9780×10^{-12}
h_K	0.1262×10^{-8}	0.1094×10^{-8}
h_{KJ}	-0.841×10^{-11}	-0.841×10^{-11}
L_K	-0.428×10^{-12}	-0.428×10^{-12}

Note. The results are in cm^{-1} .

[a] Rotational constants of *Cis*-HONO from Dehayem-Kamadjeu *et al.* [13]
For the 4^1 upper state, the constants were slightly readjusted using the upper and lower states constants from Ref. [12] and the updated ground state parameters from Ref. [13] (see text).

Table 3 : results of the present line intensity and position computation at 296K

Conformer	Nb	Sig_min	Sig_max	Int_Max[#]	Total_Int[#]
Trans- HONO	7621	724.39	838.57	0.166	$^{Trans}Int(\nu_4,T)= 1.218$
Cis-HONO	18420	722.53	996.28	0.148	$^{Cis}Int(\nu_4,T)= 1.249$
Total	26041				$Int(\nu_4,T)=2.467$

All lines (Trans- and Cis-)	Sigma < 820 cm^{-1}	Sigma > 820 cm^{-1}	11 μm
Sum of the individual intensities[#]	$^{\sigma<820}Int(\nu_4,296K)$ [#]	$^{\sigma>820}Int(\nu_4,296K)$) [#]	$Int (\nu_4,296K)$ [#]
Calculation (This work)	1.26	1.21	2.47
Integrated band intensities[£]	$^{\sigma<820}S(296K)$ [#]	$^{\sigma>820}S(296K)$ [#]	$S(11μm,296K)$[#]
Computed (this work)[¥, £]	1.46	1.40	2.87
PNNL[£] [10]	1.44	1.40	2.84

Caption:

Nb: number of lines

Sig_Min, Sig_Max; minimum and maximum sigma values (in cm^{-1}).

$^{\#}$All intensities are given in 10^{-17}cm^{-1}/(molecule.cm^{-2}) at 296K.

Total Int: ^{Trans}Int(ν_4,T), ^{Cis}Int(ν_4,T) and Int(ν_4,T)=^{Trans}Int(ν_4,T)+^{Cis}Int(ν_4,T) : sum of the individual intensities for the Trans- and Cis- insomers and for both isomers, respectively.

Int_Max : Maximum intensity. The intensity threshold limit is Int_Min= 0.5×10-24 cm^{-1}/(molecule.cm^{-2}).

Total int: sum of the individual intensities for the Trans and Cis forms, ^{Trans}Int(ν_4,T=296K) and ^{Cis}Int(ν_4,T=296K), respectively.

Sigma < 820 cm^{-1}, Sigma > 820 cm^{-1}, and 11 μm: sum of the individual line intensities (Int(ν_4,296K)) or integrated band intensities (S(11μm,296K)) in the 720-820 cm^{-1}, 820-1000 cm^{-1} and in the full 11 μm region (720-1000 cm^{-1}), respectively. The 820 cm^{-1} cutoff is defined in Eq.(8).

$^{¥}$The computed integrated band intensities are deduced from $^{\sigma<820}$Int(ν_4,296K), $^{\sigma>820}$Int(ν_4, 296K), and Int(ν_4,296K) by a multiplication by Z_{Vib}(296K)=1.1615 (see Eq. 23).
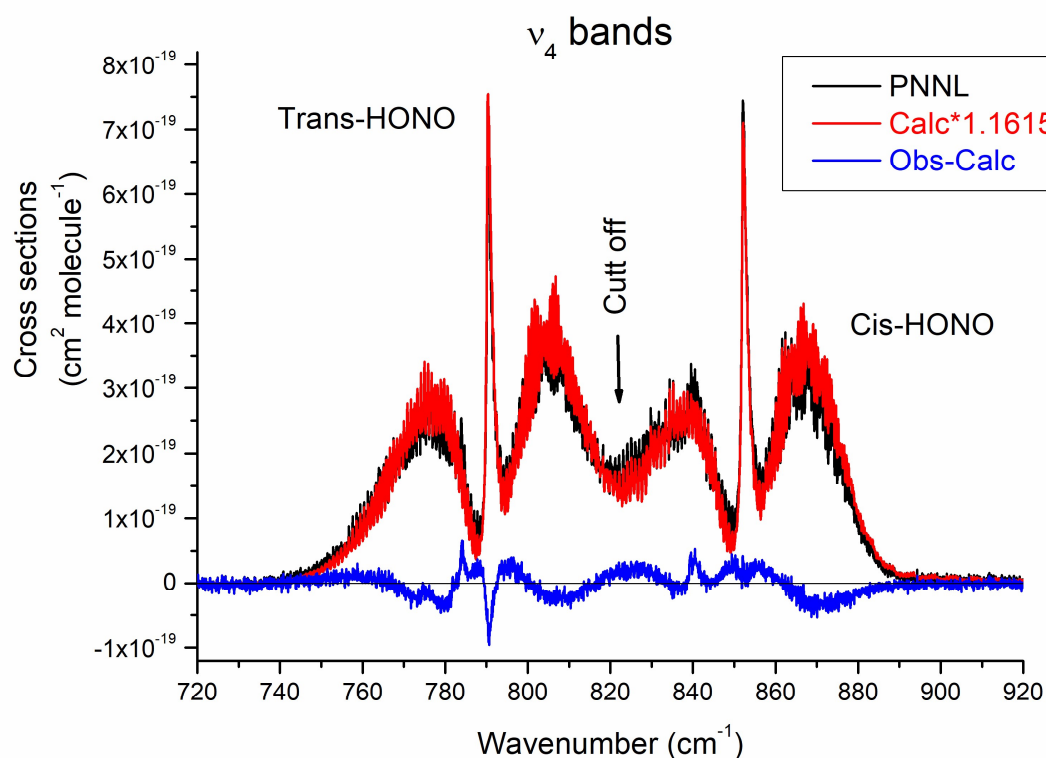
List of figures

Figure 1: Comparison between the PNNL cross sections and the results of the present computation at T=296K. This calculation is performed for HONO diluted in an atmosphere of nitrogen and for γ_{Air}=0.1 cm^{-1}/Atm. For an easier comparison, the calculated cross sections (this work) are multiplied by the mean (Trans and Cis HONO) vibrational partition function Z_{Vib}(296k)=1.1615 to account for the hot bands contributions. This calculation is performed for HONO diluted in an atmosphere of nitrogen and for γ_{Air}=0.1 cm^{-1}/Atm. More detailed informations on the experimental conditions for HONO are defined in the PNNL document [10] and in the text.
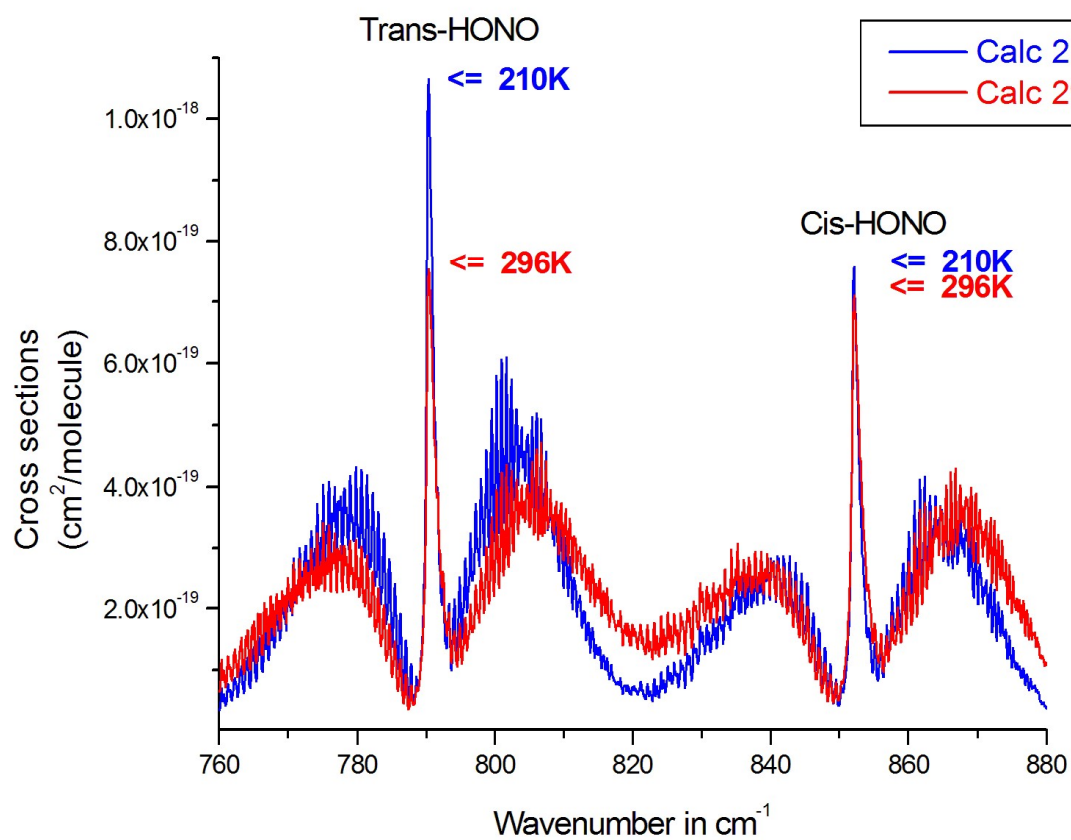
Figure 2: Computed cross sections calculated using the present linelist for the ν_4 bands of Trans- and Cis-HONO at T=296K and at T=210K. These calculations were performed for the same HONO concentration than in Fig. 1. It is clear that the relative contribution of the Cis- form to the HONO signature at 11 μm relative to the Trans- one is significantly weaker at low temperatures.
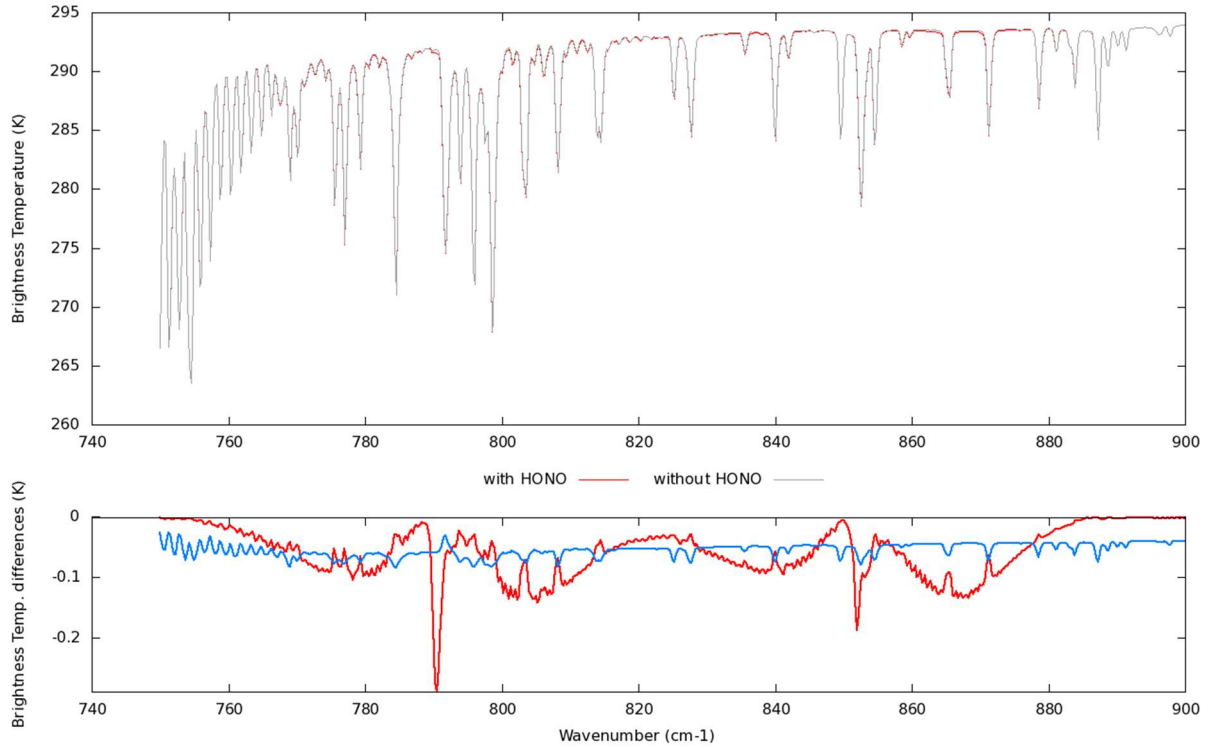
Figure 3: Simulation in brightness temperature (K) of a HONO signature on a IASI spectra. This computation was performed for a total content of HONO of 1.03 ppbv and for a mean tropical atmosphere and using the 4A/OP radiative transfer code. On the top is represented the spectra with (in red) or without HONO (in grey). Below is represented respectively, in red the Brightness Temperature difference (Brightness Temp. differences) in K between the two simulations and in blue the sensitivity to a variation of 1% of water vapor, the main pollutant in the spectral region of HONO.
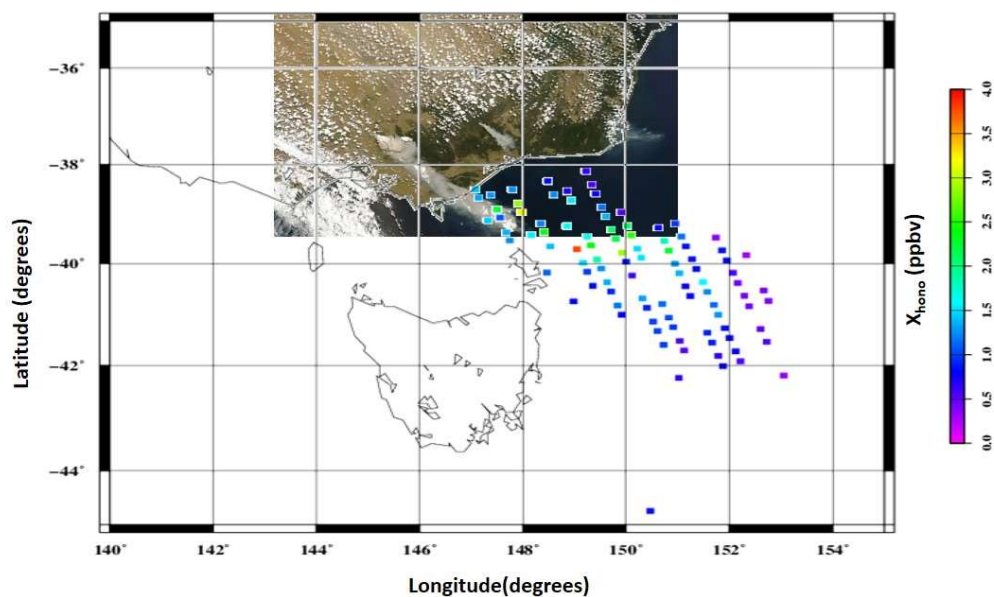
Figure 4 : True color imagery from the US MODIS Aqua satellite passes around 04 UTC (7 February, 3 PM EDT) on Saturday 7 February 2009 showing the smoke plumes from fires, including the dense cloud column ascending to high altitudes from the Kilmore fire (Image courtesy of MODIS Rapid Response Project at NASA/GSFC). The X_{HONO} inversions points (colored squares) performed for the IASI instrument (9:30 PM) on the same day, are over plotted in the range 0 to 4 ppbv and for a zone in latitude and longitude over the south of Australia and the Tasmania island.